Science of the Total Environment 669 (2019) 1043–1052

Contents lists available at ScienceDirect

Science of the Total Environment

journal homepage: www.elsevier.com/locate/scitotenv

Growing season extension affects ozone uptake by European forests

Alessandro Anav [a,b,*], Alessandra De Marco [b], Pierre Friedlingstein [c], Flavia Savi [d], Pierre Sicard [e], Stephen Sitch [f], Marcello Vitale [g], Elena Paoletti [a]

[a] National Research Council, Sesto Fiorentino, Italy
[b] Italian National Agency for New Technologies, Energy and the Environment (ENEA), Climate Modeling Laboratory, S. Maria di Galeria, Rome, Italy
[c] University of Exeter, College of Engineering, Mathematics and Physical Sciences, Exeter, UK
[d] Council for Agricultural Research and Economics, Research Centre for Forestry and Wood, Arezzo, Italy
[e] ARGANS, Sophia Antipolis Cedex, France
[f] University of Exeter, College of Life and Environmental Sciences, Exeter, UK
[g] University of Rome "Sapienza", Department of Environmental Biology, Rome, Italy

HIGHLIGHTS

- Surface ozone concentrations have reduced 1.6% from 2000 to 2014 in Europe.
- Trends for two metrics used for risk assessment, the AOT40 and POD_Y, have been computed.
- AOT40 declined 22% while PODY increased 6%.
- Climate change lengthened the growing season (~7 days/decade) thus enhancing POD_Y.
- POD_Y is a more climatologically-relevant ozone metric than AOT40.

GRAPHICAL ABSTRACT

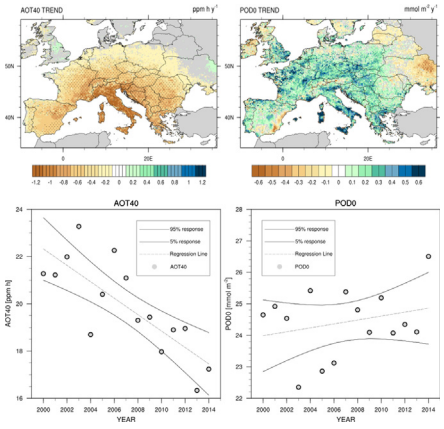

ARTICLE INFO

Article history:
Received 15 January 2019
Received in revised form 1 March 2019
Accepted 2 March 2019
Available online 14 March 2019

Keywords:
Tropospheric ozone
Climate change
Forests
POD
AOT40

ABSTRACT

Climate change significantly modifies terrestrial ecosystems and vegetation activity, yet little is known about how climate change and ozone pollution interact to affect forest health. Here we compared the trends of two metrics widely used to protect forests against negative impacts of ozone pollution, the AOT40 (Accumulated Ozone over Threshold of 40 ppb) which only depends on surface air ozone concentrations, and the POD (Phytotoxic Ozone Dose) which relies on the amount of ozone uptaken by plants through stomata. Using a chemistry transport model, driven by anthropogenic emission inventories, we found that European-averaged ground-level ozone concentrations significantly declined (−1.6%) over the time period 2000–2014, following successful control strategies to reduce the ozone precursors emission; as a consequence, the AOT40 metric declined (−22%). In contrast, climate change increased both growing season length (~7 days/decade) and stomatal conductance and thus enhanced the stomatal ozone uptake by forests (5.9%), leading to an overall increase of potential ozone damage on plants, despite the reduction in ozone concentrations. Our results suggest that stomatal-flux based strategies of forest protection against ozone in a changing climate require a proper consideration of the duration of the growing season with a better estimation of start and end of the growing season.

© 2019 Elsevier B.V. All rights reserved.

* Corresponding author at: National Research Council, Sesto Fiorentino, Italy.
E-mail address: alessandro.anav@ipsp.cnr.it (A. Anav).

https://doi.org/10.1016/j.scitotenv.2019.03.020
0048-9697/© 2019 Elsevier B.V. All rights reserved.

1. Introduction

Climate change modifies the functioning of terrestrial ecosystems leading to increased primary production (Nemani et al., 2003), growth (Myneni et al., 1997) and greening (Zhu et al., 2016) of plants. In contrast, tropospheric ozone (O_3) damages both forests and crops reducing primary production (Sitch et al., 2007; Wittig et al., 2009) and crop yield (Ashworth et al., 2013; Avnery et al., 2011). Tropospheric ozone is a secondary air pollutant, formed by reactions among precursors, in particular nitrogen oxides (NO_x) and non-methane volatile organic compounds (NMVOC), in the presence of sunlight (Madronich, 2014; Monks et al., 2015). These primary pollutants originate from human activities, such as oil and coal combustion, and from natural emissions from plants.

To assess the potential O_3 damages to vegetation several metrics have been developed (Musselman et al., 2006; Paoletti and Manning, 2007). The European standard is AOT40, i.e. the accumulation of O_3 concentrations exceeding 40 ppb over daylight hours (8 AM–8 PM) from May to July (EU directive 2008/50/EC). However, AOT40 has one major limitation (Fuhrer et al., 1997; Ashmore et al., 2004): it assumes that the damage to vegetation depends on the above canopy O_3 concentration, while O_3 damages plants only when it enters the leaves through the stomata (Paoletti and Manning, 2007). For this reason, a new metric has been proposed to replace AOT40: the Phytotoxic Ozone Dose (POD_Y), defined as the accumulated O_3 flux entering the leaves via the stomata over a detoxification threshold (Y) (Emberson et al., 2000; Paoletti and Manning, 2007), which summarizes the role of environmental and plant factors in affecting the stomatal uptake of O_3.

How the O_3 threat to forests is affected by the interaction between climate change and air pollution is not well established (Sicard et al., 2016a). Many studies compared O_3 risk assessment based on either AOT40 or POD_Y, and highlighted spatial and temporal (i.e. inter-annual variability) inconsistencies between these two metrics (Simpson et al., 2007; Mills et al., 2011; Anav et al., 2016; De Marco et al., 2016; Sicard et al., 2016b). Few studies compared AOT40 and POD_Y trends over recent climate change, and all of them were carried out at individual forest sites. Araminienė et al. (2019) used the WFR-CHIMERE multi-model system and found a reduction of AOT40 and an increase of POD_0 at nine forest sites in Lithuania over 2007–2014. At eight sites in Fennoscandia and northern UK over 1990–2015, Karlsson et al. (2017) found a significant reduction in AOT40 and no change in the POD_1 of *Picea abies*. Klingberg et al. (2014) analyzed the changes in AOT40 and POD_1 of *Picea abies* at 14 EMEP monitoring sites finding a reduction in both metrics between the periods 1990–2009 and 2040–2059, mainly explained by reduced emissions of O_3 precursors and thus O_3 concentrations. Hendriks et al. (2016) estimated the effects of future climate change (2050 vs. 2010) on POD_1 of deciduous trees across Europe by using the LOTUS-EUROS model, and did not find significant changes. Klingberg et al. (2011) investigated the influence of climate change on simulated POD_Y of a generic crop and a generic deciduous tree at ten European sites. Despite substantial increase in future O_3 concentrations in central and southern Europe, they predicted that the flux-based risk for O_3 damage to vegetation will remain unchanged or decrease at most sites, mainly as a result of projected reductions in stomatal conductance under rising CO_2 concentrations and drier conditions (Klingberg et al., 2011).

To provide a full picture of the effect of climate change on O_3 uptake by forests in Europe (excluding Fennoscandia), the aims of this study were to assess: 1) whether the reduction of O_3 precursors in Europe has been effective in reducing the risk of O_3 injury all across the actual European forests over the time period 2000–2014; 2) whether the risk was affected by climate change, and 3) which environmental (O_3 concentrations, air temperature, vapour pressure deficit, soil water content) and plant-related variables (phenology) were the main drivers of the changes in stomatal ozone flux induced by climate change. To address these questions, we compared spatial AOT40 and POD_Y trends over time (POD_0 and POD_1 with a threshold of 0 and 1 nmol m^{-2} s^{-1}, respectively) using modeled data. We hypothesized that: 1) O_3 concentrations and AOT40 declined from 2000 to 2014, while POD_Y did not; and 2) climate change markedly affects POD_Y through a longer growing season. Anav et al. (2017) demonstrated that plant phenology has a significant impact on the estimation of stomatal O_3 flux magnitude. Compared to previous trend studies, here we improved the definition of POD_Y by considering a complex phenological model used to extract the growing season length.

2. Methods

2.1. Atmospheric chemistry modelling

The model used in this study to reproduce surface O_3 concentrations was CHIMERE (v2013b); it is an Eulerian chemistry-transport model developed to simulate gas-phase chemistry, aerosol formation, transport and deposition at regional scale (Menut et al., 2013). In our configuration CHIMERE had a spatial resolution of 12 km with 8 hybrid-sigma vertical levels extending from surface to 500 hPa. We ran the model from 01 December 1999 to 31 December 2014 using the first month as spin up. A 15-year simulation ensures to see changes in surface gas concentrations (Sicard et al., 2009; Monks et al., 2015). Meteorological fields required by CHIMERE, and also used in our analysis to estimate the O_3 risk for forests, were provided by the WRF (v3.6) model (Skamarock et al., 2008), with a horizontal resolution of 12 km. The initial and boundary meteorological conditions for WRF model were provided by the European Centre for Medium-range Weather Forecast (ECMWF) analyses with a horizontal resolution of 0.7° every 6 h. Yearly EMEP emission inventory (Mareckova et al., 2014) was used for the anthropogenic emissions; it includes all human activities, like traffic, industries, and agriculture. Biogenic emissions are directly computed by CHIMERE through the MEGAN model (Guenther et al., 2006; Guenther et al., 2012).

A detailed comparison of simulated meteorological variables and O_3 concentrations with observations is given in supporting information.

2.2. Forest impacts

Ozone threat to forests was estimated using two metrics. In order to facilitate the comparison between the two metrics, AOT40 was computed according with its revised formulation (Anav et al., 2016), i.e. as the sum of the hourly exceedances above 40 ppb computed over the year when stomata are open:

$$AOT40 = \begin{cases} \int_{t=01-Jan}^{31-Dec} \max([O_3]-40,0)dt; g_{sto}>0 \\ 0; g_{sto}=0 \end{cases} \quad (1)$$

where $[O_3]$ is the hourly O_3 concentration (ppb), dt is the time step (1 h) and g_{sto} is the stomatal conductance to O_3 based on the Projected Leaf Area (PLA) and computed using the DO_3SE model (see Supporting information).

The second metric was POD_Y, i.e. POD over a detoxification threshold (Y), with Y equal to either 0 nmol m^{-2} PLA s^{-1} (because of the lack of information on the amount of O_3 in the mesophyll that is detoxified without inducing any injury) or 1 nmol m^{-2} PLA s^{-1} (as suggested by UNECE, 2017). POD_0 was computed according to the DO_3SE model by Emberson et al. (2000):

$$POD0(t) = \int_{t=01-Jan}^{t=31-Dec} \left([O_3] * g_{sto} * \frac{R_c}{R_b + R_c}\right) dt \quad (2)$$

where R_b represents the quasi-laminar resistance and R_c the leaf surface resistance (Simpson et al., 2007; Tuovinen et al., 2007; Büker et al., 2015) and g_{sto} is the stomatal conductance computed as following:

$$g_{sto} = g_{\max} * f_{phen} * f_{light} * \max\left(f_{\min}, f_{temp} * f_{VPD} * f_{SWC}\right) \quad (3)$$

where g_{max} is the maximum stomatal conductance of a plant species to O_3 (Anav et al., 2016), and f_{min} is the minimum stomatal conductance expressed as a fraction of g_{max}. The f_{temp}, f_{light}, f_{VPD}, and f_{SWC} are functions varying between 0 and 1, with 1 meaning no limitation to stomatal conductance; they describe the variation of g_{max} with surface air temperature (T, °C), photosynthetic photon flux density ($PPFD$, μmol photons $m^{-2}\,s^{-1}$), vapour pressure deficit (VPD, kPa) estimated through the surface air humidity, and volumetric soil water content (SWC, $m^3\,m^{-3}$), respectively (see Supporting information). The parameterization of the different forest types was the same as in Anav et al. (2016). The spatial distribution of the dominant forest types was based on the European Forest Institute (EFI) data (Tröltzsch et al., 2009; Brus et al., 2011), converted to the DO_3SE categories (UNECE, 2017) by using the European Environmental Agency (EEA) biogeographic regions (Anav et al., 2016).

Similarly to POD_0, the POD_1 was computed as following:

$$POD1(t) = \int_{t=01-Jan}^{t=31-Dec} \max\left([O_3] * g_{sto} * \frac{R_c}{R_b + R_c} - 1, 0\right) dt \quad (4)$$

Details on the validation of stomatal conductance estimates are in the Supporting information. To attribute the trend in POD_Y to the variables regulating the stomatal opening, we computed POD_Y with only one driving variable varying during the 2000–2014 time period, while the other variables are fixed at their climatological mean, and we calculated the relative percent change of POD_Y.

2.3. Plant phenology

To define the start (SOS) and end (EOS) of the growing season, the DO_3SE model applies a simple latitude model (UNECE, 2017); however, this latitude model uses a fixed time window for the O_3 accumulation, hence it does not consider any potential influence of climate change on the duration of the growing season (Piao et al., 2007, 2015) and thus of the period during which plants can uptake O_3.

Normalized Difference Vegetation Index (NDVI) serves as a proxy of vegetation activity. Based on the results by Anav et al. (2017), we adopted the biweekly composited GIMMS $NDVI_{3g}$ data (Pinzon and Tucker, 2014) with spatial resolution of 0.1 × 0.1° to extract the date

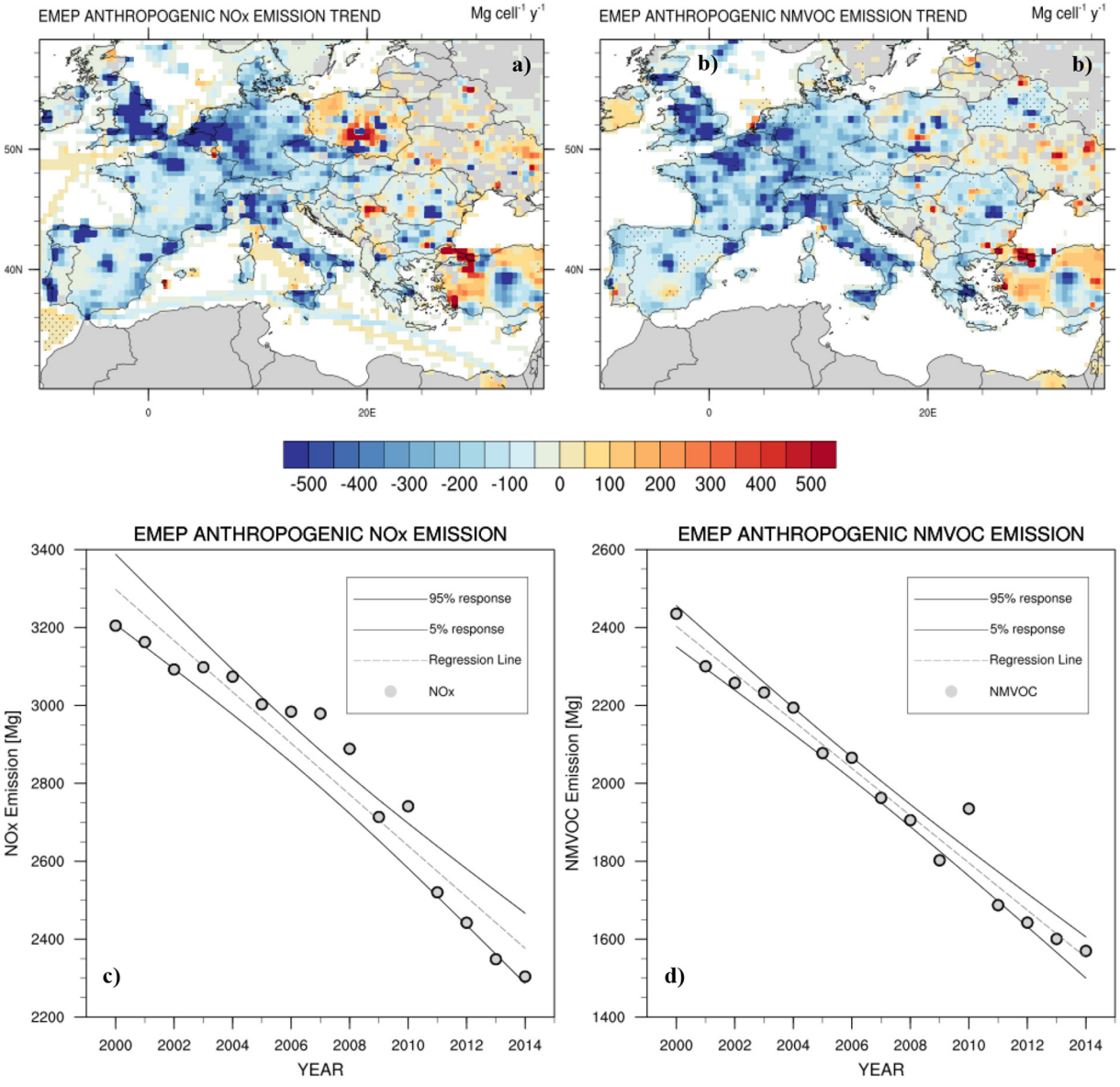

Fig. 1. Spatial distribution of anthropogenic emissions trends computed using linear least fit square of annual total over the time period 2001–2014 for (a) NOx and (b) NMVOC. Stipples indicate trends that are statistically significant at 95% confidence level (two tailed t-test). c, d, Year-to-year variability of (c) NOx and (d) NMVOC emissions averaged over the whole domain along with regression lines and 95% confidence interval.

of SOS and EOS. Pixels probably influenced by snow coverage during non-growing season were screened out and replaced by NDVI of the temporally nearest snow-free date (Liu et al., 2016a, 2016b; Anav et al., 2017). This also restricted the estimated SOS/EOS from going beyond thermal growing season. We first calculate the NDVI ratio from 15-year averaged NDVI time-series to determine the NDVI thresholds with maximum and minimum change of $NDVI_{ratio}$ for SOS and EOS, respectively.

$$NDVI_{ratio}(t) = [NDVI(t+1) - NDVI(t)]/[NDVI(t)] \quad (5)$$

Then, we fit the biweekly sampled NDVI data to a function of Julian day (x in the following equation) through a six-degree polynomial function (Piao et al., 2006; Liu et al., 2016a, 2016b).

$$NDVI = a + a_1x^1 + a_2x^2 + a_3x^3 + \ldots + a_6x^6 \quad (6)$$

2.4. Trend analysis

Trends were computed at each grid point by using yearly estimates. For each point, the slope was computed by a standard linear least square method and the significance of the trend was assessed with a two tailed *t*-test at 95% confidence level. In addition, Mann-Kendall non-parametric trend analyses were conducted to determine the statistical significance of any observed trends and the Sen's slope statistics were calculated with confidence intervals.

To assess the percentage of change between chemical variables from the beginning to the end of our temporal period, relative trends (in %/year units) were also estimated following the methodology of the EMEP trend report (Colette et al., 2016). The relative trends (R_t) were computed using as reference the estimated value from the linear least square method at the first year of analysis (y_0, i.e. 2000):

$$R_t = 100\frac{a}{y_0} \quad (7)$$

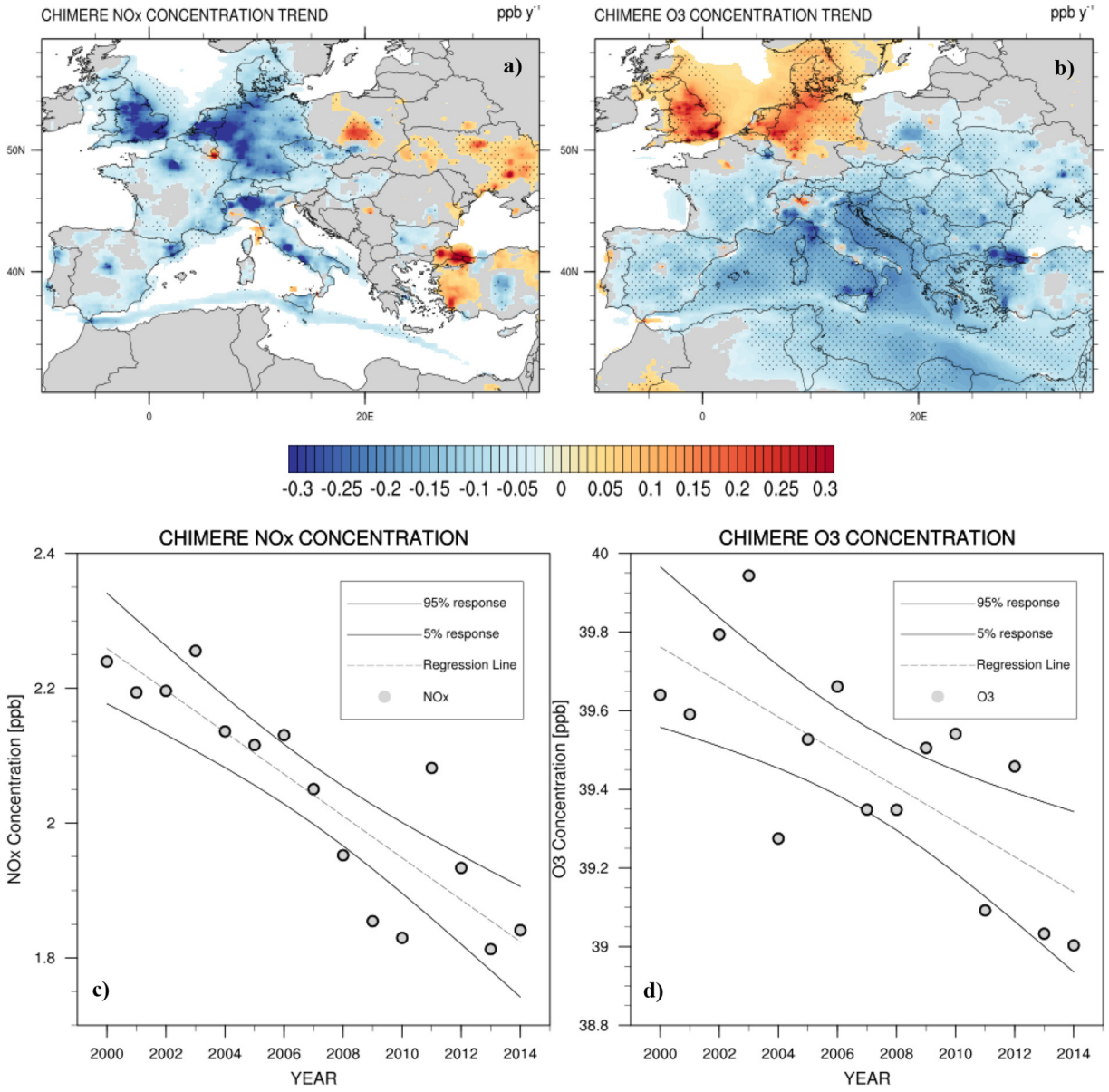

Fig. 2. Spatial distribution of simulated (a) [NOx] and (b) [O_3] trends computed using linear least fit square of annual total over the temporal period 2001–2014; stipples indicate trends that are statistically significant at 95% confidence level (two tailed *t*-test). c, d, Interannual variability of (c) NOx and (d) O_3 concentrations averaged over the only land points of the domain along with regression lines and 95% confidence interval.

where a represents the slope of the linear fit estimated by the Sen's method. The use of the estimated value at the start allows using a reference that is less sensitive to inter-annual variability than the actual observed value at t_0 (Colette et al., 2016). Finally, to assess the relative change over a given time span, the relative annual trend over the period was multiplied by the number of years during that period minus one.

3. Results

The European emissions control strategies were effective in reducing O_3 precursor emissions: NOx and NMVOC emissions, used to drive our model, showed a significant widespread negative trend (Fig. 1a–b), except for a few isolated locations in Turkey and Eastern Europe.

The overall changes in the annual European-averaged NO_x and NMVOC emissions indicated a statistically significant decrease ($p < 0.01$) of 61.4 Mg/yr and 56.7 Mg/yr, respectively, corresponding to a reduction of 27.9% and 35.4% over the time period 2000–2014 (Fig. 1c-d). Our chemistry transport model indicated that the decrease of anthropogenic emissions led to a reduction of mean daily surface NO_x concentration over central Europe (Fig. 2a), reflecting the trend of primary emissions reported in the inventory. In contrast, surface O_3 showed a twofold spatial pattern (Fig. 2b): in Southern Europe there was a negative trend, while in England and central-northern Europe, where NO_x and NMVOC emissions were strongly reduced (Fig. 1a–b), the O_3 trend was positive. Averaged over the domain, both NO_x and O_3 showed a significant decrease in surface concentration ($p < 0.01$) of −0.029 ppb/yr and −0.04 ppb/yr, respectively (Fig. 2c–d), corresponding to a reduction of 19.2% and 1.6% from 2000 to 2014.

According to the overall O_3 reduction, AOT40 showed a decline all over Europe with the highest and most significant reductions (up to -1.2 ppm h y^{-1}) in Southern Europe (Fig. 3a). Although over central Europe we found increasing O_3 concentrations (Fig. 2b), AOT40 showed a negative trend of −0.32 ppm h yr^{-1} (Mann–Kendall test, $p < 0.1$), corresponding to a reduction of 22% over the 2000–2014 time period (Fig. 3c).

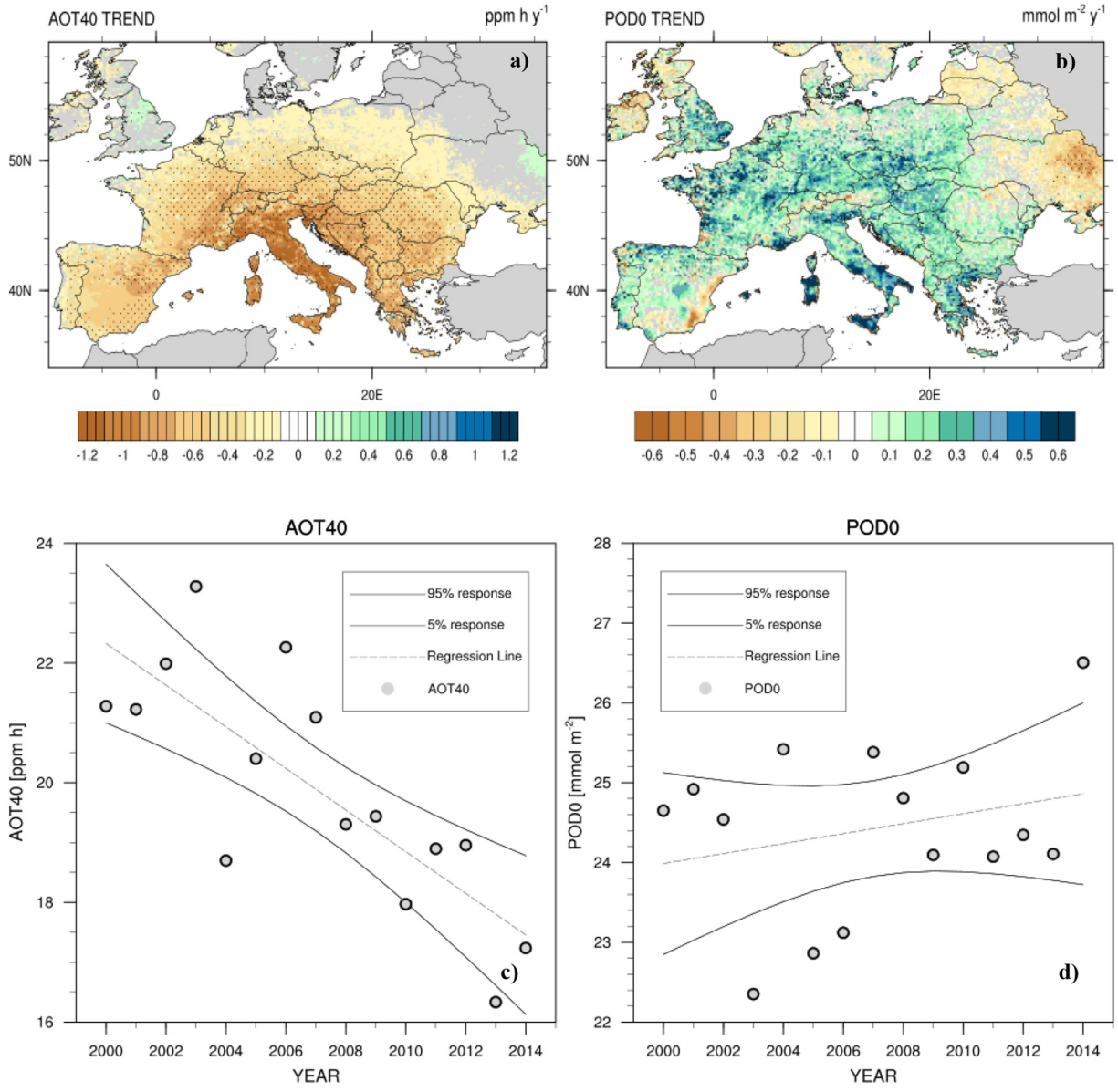

Fig. 3. Spatial pattern of (a) AOT40 and (b) POD0 trends computed using linear least fit square of annual total over the temporal period 2001–2014; stipples indicate trends that are statistically significant at 95% confidence level (two tailed t-test). c, d, Yearly variability of (c) AOT40 and (d) POD0 averaged over the domain along with regression lines and 95% confidence interval.

Unlike AOT40 which decreased over large areas of the domain, the POD_0 spatial distribution showed slightly increasing trends over most of Europe (Fig. 3b). We found a European-averaged POD_0 trend of 0.1 mmol yr^{-1} (Mann–Kendall test, $p < 0.1$), corresponding to an increase of 5.9% over 2000–2014 (Fig. 3d). Because of a lack of consensus about the Y detoxification threshold for forest protection, we also computed POD_1 trends in addition to POD_0. The spatial and temporal variations of POD_1 were in perfect agreement with the variations of POD_0, while the absolute values of POD_1 were around 4 times lower than the POD_0 ones; we found a European-averaged POD_1 variation of 0.03 mmol yr^{-1} (Mann–Kendall test, $p < 0.1$), corresponding to an increase of 7.3% over the time period 2000–2014.

To explain the positive POD_Y trends, we investigated the individual components regulating the stomatal opening (Eq. (3)). Consistent with other studies (e.g. Zeng et al., 2011; Shen et al., 2014), we found that the mean dates of vegetation green-up advanced at a rate of 3.2 days/decade between 2000 and 2014 (Fig. 4a). This earlier SOS trend was caused by a warmer trend in the mean February–March–April temperature of 0.16 °C/decade (Fig. S6). Similarly, the mean date of vegetation senescence showed a delay of 4.9 days/decade (Fig. 4b) caused by a warmer trend in fall temperature of 0.7 °C/decade (Fig. S6). Overall, over the study area the mean annual air temperature increased by 0.29 °C/decade, leading to a longer growing season (+~7 days/decade) and thus a longer period during which plants are susceptible to uptake O_3. The spatial distribution of the trends of the limiting functions indicated a reduced limitation (i.e. more favorable conditions for stomata opening) for air temperature, relative humidity and soil moisture, while the function describing the role of radiation displayed a higher limitation (Fig. 4c–f). This is consistent with ongoing climate change, namely an increase in mean annual air temperature generates higher

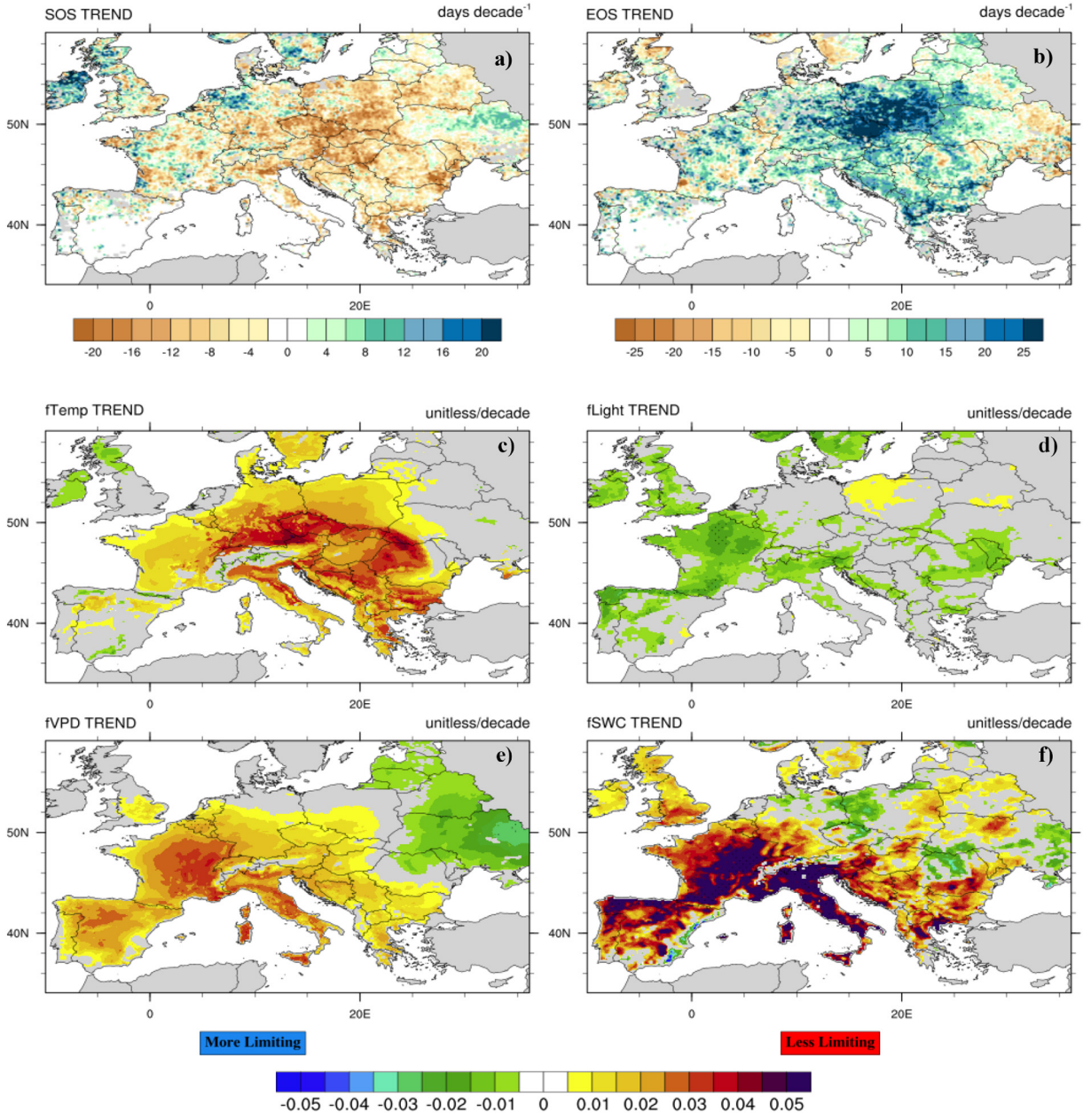

Fig. 4. Spatial distribution of trends in (a) dates of vegetation green-up (SOS) and (b) vegetation senescence (EOS). c, d, e, f, Trends of functions limiting the stomatal uptake and describing the decrease of maximum stomatal conductance with (b) air temperature (c) radiation (d) air humidity and (e) soil water content. Stipples indicate trends that are statistically significantly at 95% confidence level (two tailed *t*-test).

evaporation and air humidity, more clouds and thus reduces the downward short-wave radiation, producing finally more precipitation and a higher soil moisture.

Considering the mean annual cycle of the meteorological limiting functions averaged over the whole domain, our results suggest that stomatal uptake of O_3 was limited by low temperature and irradiance during winter, while soil moisture was the main limiting factor during warmer months (Fig. 5a). The monthly limitation of each meteorological variable to stomatal conductance (Fig. 5b–e) suggests that the stomatal opening above 40 N of latitude during January–February–March and November–December was mainly regulated by surface air temperature and marginally by radiation at high latitudes, while soil moisture did not exhibit a strong limitation. Conversely, during summer and mainly in the Mediterranean basin (below 44°N of latitude), the stomatal opening was limited by low soil moisture and relative humidity, and high temperature.

Finally, to attribute the trend in POD_0 to the variables regulating stomatal opening, we found that POD_0 increased primarily because of the trend in phenology (+5.1%), soil moisture (+2.8%), temperature (+2.2%) and air humidity (+1.1%), while the trend in O_3 alone would lead to a decrease of POD_0 by 4.0% (Fig. 6). Similarly, the trend in radiation led to a reduction of POD_0 by 0.8%.

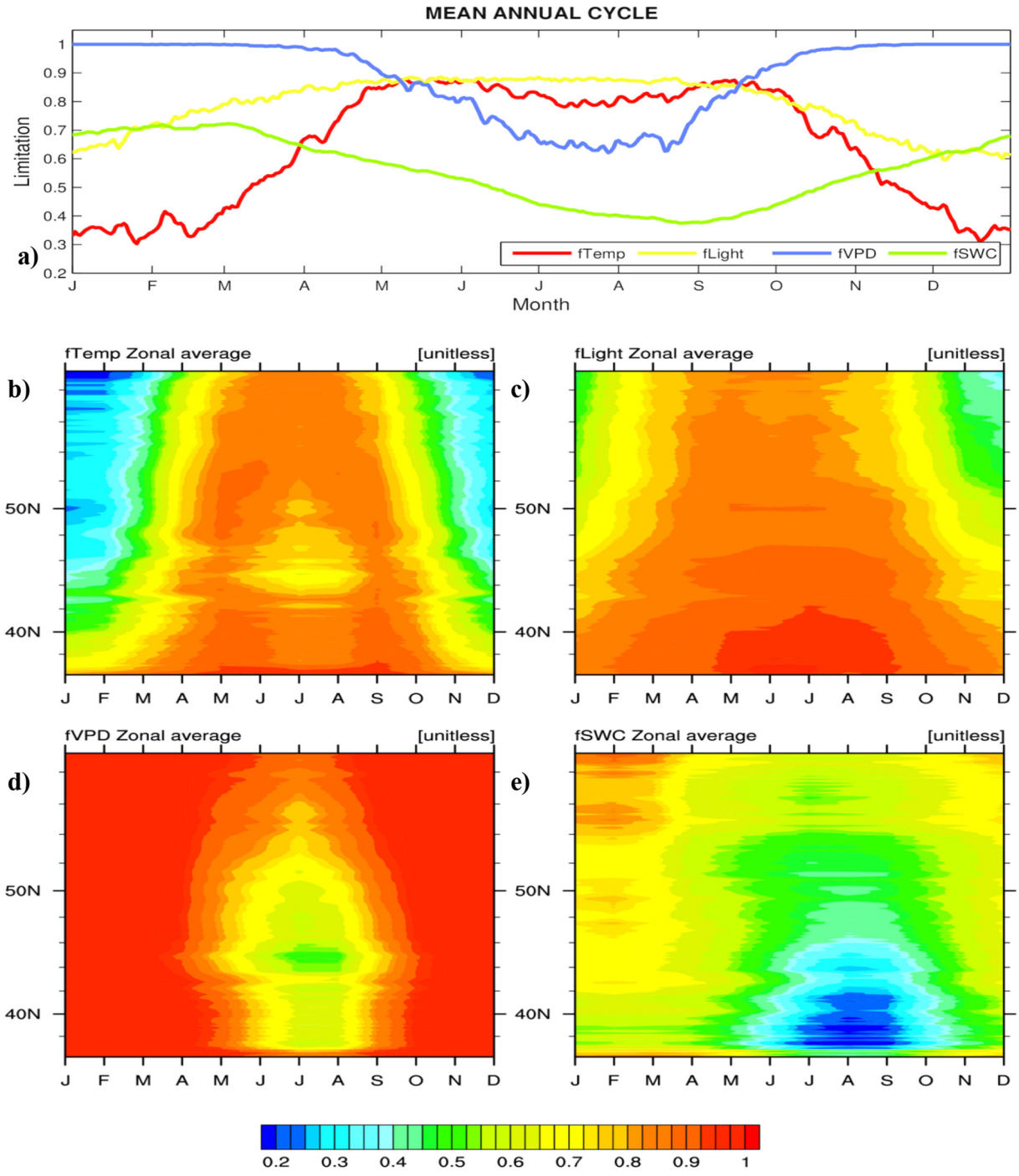

Fig. 5. Mean annual cycle of the limiting functions averaged over the domain (0 fully limited; 1 no limitation) describing the effects of air temperature (fTemp), solar radiation (fLight), vapour pressure deficit (fVPD) and soil water availability (fSWC) on stomatal functioning (a) along with their zonally-averaged climatologies computed using monthly values over the temporal period 2000–2014 (b–e).

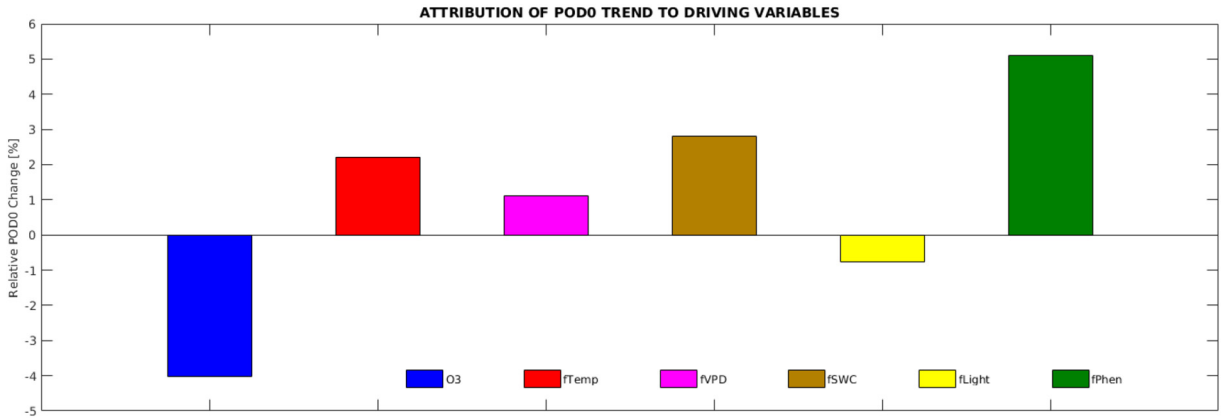

Fig. 6. Attribution of POD_0 trend to variables regulating the stomatal uptake of O_3. Each bar represents the change in POD_0 with only one driving variable varying during the 2000–2014 time period, while the other variables are fixed at their climatological mean.

4. Discussion

Findings of the present study confirmed that, despite O_3 has reduced from 2000 to 2014 following successful control strategies to reduce the emission of NOx and NMVOC precursors, it still represents a problem for the protection of European forests. Interestingly, O_3 concentrations decreased in Southern Europe and increased over England and central-northern Europe, suggesting that over these latter regions the reduction of anthropogenic emissions was insufficient to change the chemical regimes from VOC-sensitive to NO_x-sensitive (Beekmann and Vautard, 2010) thus leading to a predominant role of reduced night-time titration of O_3 as a result of NO_x decrease (Colette et al., 2011).

Although O_3 concentrations increased over central Europe, AOT40 showed a negative trend. This result was not unexpected: in fact, while O_3 trends are computed from daily averages, only daytime hours are used for AOT40, suggesting that the decrease in NO_x and NMVOC emissions led to a reduction of daytime O_3 maxima and an increase in nighttime concentrations (Sicard et al., 2016c; Karlsson et al., 2017). This latter is a consequence of the longer lifetime of O_3 due to reduced availability of NO_x (Colette et al., 2011). In addition, it should be noted that the changes in plant phenology, which promote increasing POD trends, do not affect AOT40 trends: this is related to the fact that concentrations below 40 ppb (typical of early spring and late autumn and coincident with green up and dormancy dates) do not contribute to the final value of the metrics. In other terms, the O_3 concentrations found at the beginning (end) of the growing season do not exceed the threshold used by the AOT40 (i.e. 40 ppb) and thus they do not contribute to the final value of the metric and hence to its trend.

The magnitude of our AOT40 trend (i.e. -22%) was in agreement with a previous study in Europe suggesting that AOT40 has reduced by 0.226 ppm h yr^{-1} from 2002 to 2012, corresponding to a reduction of 37% (Colette et al., 2016). Similarly, a different analysis conducted at 61 rural sites in France indicates that AOT40 has reduced by 27% over the 1999–2012 time period (Sicard et al., 2016c). As we postulated, O_3 concentrations and AOT40 declined from 2000 to 2014, while POD_Y did not. This result was consistent with a recent study showing that AOT40 is projected to no longer exceed the critical level established for forest protection for most of northern Europe around the 2050, while POD_1 does not fall below this critical level (Karlsson et al., 2017). We found that the reason of the relative insensitivity of POD_Y to O_3 precursors control was climate change, in particular it lengthens the growing season (~7 days/decade) through an earlier SOS (3.2 days/decade) and delayed EOS (4.9 days/decade). This result is confirmed by several recent studies which report earlier green-up dates and delayed dormancy dates because of changing climate (Wolkovich et al., 2012; Liu et al., 2016a, 2016b; Fu et al., 2017).

Besides, we highlight how, to define SOS and EOS (i.e. the period during which plants uptake O_3 from atmosphere) the POD_Y metric uses a simple latitude model with a fixed time window for the O_3 accumulation (Anav et al., 2017). Therefore this method cannot consider the inter-annual variability in the climate system as well as the influence of the climate change on the duration of the growing season and thus of the period during which plants can uptake O_3. Here we suggested how to improve the POD_Y metric to overcome this weakness.

Our study suggests another reason why using AOT40 as a metric to control O_3 threat to forests is not appropriate as it does not account for the change of plant stomatal uptake with a changing climate. In addition to the effect of the duration of the growing season on POD_0 (+5.1%), the climatic changes in Europe had another effect on forests, i.e. a decrease of limitations to stomatal opening. The beneficial effects of higher temperature (+2.2%) and soil moisture (+2.8%) on increasing stomatal conductance offset the reduction in O_3 concentrations (−4.0%), leading to a slightly increased oxidative O_3-based stress to the European forests. This result agrees with other studies conducted at several observational sites which showed that air temperature is the most important variable influencing CO_2 and O_3 uptake by plants, while soil moisture plays a pivotal role in Mediterranean and semi-arid sites (Fares et al., 2013; Proietti et al., 2016). Although projections for the Mediterranean region showed a tendency for drier and warmer climate in the next century (Mariotti et al., 2015), recent results displayed that the precipitation during the last decades was characterized by multi-year to decadal anomalies rather than a long-term trend (Dell'Aquila et al., 2016). This precipitation pattern may explain the increasing trend in soil moisture found in our study.

We speculate that the positive feedback between climate change and POD_Y will increase in the near future and the efforts in controlling emissions of O_3 precursors could be significantly offset by climate change, thus increasing the O_3 risk for forests. It should be noted that the reduction in stomatal conductance caused by the CO_2 fertilization effect due to increasing CO_2 concentration is also an important factor for O_3 flux which needs to be considered when multi-decadal climate change and O_3 injuries are to be assessed (Klingberg et al., 2011). Given the relative short time period analyzed in this study, climate is the major driver of stomatal regulation and gas exchange with atmosphere (Anav et al., 2015). However, for multi-decadal assessment, the inclusion in the DO_3SE model of a specific function which considers the influence of increasing CO_2 on stomatal conductance or the use of process-based models would help to better estimate the changes in stomatal O_3 uptake.

We conclude that we should improve our knowledge on how forest ecosystems respond to the mutual interaction between air pollution and climate change (Sicard et al., 2016a; Tai et al., 2014). When moving

from AOT40 to POD_Y, forest protection against the negative impacts of O_3 requires strategies that integrate both climate and air quality policies (Ainsworth et al., 2012).

Acknowledgements

We wish to thank the three anonymous reviewers for their comments on this manuscript. We also acknowledge the entire EMEP and AIRBASE staffs for providing ground based O_3 data and the EMEP/MSC-W team for anthropogenic emissions database. The computing resources and the related technical support used for this work have been provided by CRESCO/ENEA-GRID High Performance Computing infrastructure and its staff (http://www.cresco.enea.it). CRESCO/ENEAGRID High Performance Computing infrastructure is funded by ENEA, the Italian National Agency for New Technologies, Energy and Sustainable Economic Development and by National and European research programs.

Financial support was from the MITIMPACT project (INTERREG V A – Italy – France ALCOTRA) and from the LIFE15 ENV/IT/000183 project MOTTLES of the European Union. This work was carried out within the IUFRO Task Force on Climate Change and Forest Health.

Appendix A. Supplementary data

Supplementary data to this article can be found online at https://doi.org/10.1016/j.scitotenv.2019.03.020.

References

Ainsworth, E.A., Yendrek, C.R., Sitch, S., Collins, W.J., Emberson, L.D., 2012. The effects of tropospheric ozone on net primary productivity and implications for climate change. Annu. Rev. Plant Biol. 63, 637–661.

Anav, A., Friedlingstein, P., Beer, C., Ciais, P., Harper, A., Jones, C., et al., 2015. Spatiotemporal patterns of terrestrial gross primary production: a review. Rev. Geophys. 53, 785–818.

Anav, A., De Marco, A., Proietti, C., Alessandri, A., Dell'Aquila, A., Cionni, I., et al., 2016. Comparing concentration-based (AOT40) and stomatal uptake (PODY) metrics for ozone risk assessment to European forests. Glob. Chang. Biol. 22, 1608–1627.

Anav, A., Liu, Q., De Marco, A., Proietti, C., Savi, F., Paoletti, E., et al., 2017. The role of plant phenology in stomatal ozone flux modelling. Glob. Chang. Biol. 24, 235–248.

Araminienė, V., Sicard, P., Anav, A., Agathokleous, E., Stakėnas, V., De Marco, A., Varnagirytė-Kabašinskienė, I., Paoletti, E., Girgždienė, R., 2019. Trends and interrelationships of ground-level ozone metrics and forest health in Lithuania. Sci. Total Environ. 685, 1265–1277.

Ashmore, M., Emberson, L., Karlsson, P.E., Pleijel, H., 2004. New directions: a new generation of ozone critical levels for the protection of vegetation in Europe. Atmos. Environ. 38, 2213–2214.

Ashworth, K., Wild, O., Hewitt, C., 2013. Impacts of biofuel cultivation on mortality and crop yields. Nat. Clim. Chang. 3, 492–496.

Avnery, S., Mauzerall, D.L., Liu, J., Horowitz, L.W., 2011. Global crop yield reductions due to surface ozone exposure: 2. Year 2030 potential crop production losses and economic damage under two scenarios of O_3 pollution. Atmos. Environ. 45, 2297–2309.

Beekmann, M., Vautard, R., 2010. A modelling study of photochemical regimes over Europe: robustness and variability. Atmos. Chem. Phys. 10, 10067.

Brus, D.J., Hengeveld, G.M., Walvoort, D.J.J., Goedhart, P.W., Heidema, A.H., Nabuurs, G.J., Gunia, K., 2011. Statistical mapping of tree species over Europe. Eur. J. For. Res. 131, 145–157.

Büker, P., Feng, Z., Uddling, J., Briolat, A., Alonso, R., Braun, S., et al., 2015. New flux based dose–response relationships for ozone for European forest tree species. Environ. Pollut. 206, 163–174.

Colette, A., Granier, C., Hodnebrog, Ø., Jakobs, H., Maurizi, A., Nyiri, A., et al., 2011. Air quality trends in Europe over the past decade: a first multi-model assessment. Atmos. Chem. Phys. 11, 11657–11678.

Colette, A., Aas, W., Banin, L., Braban, C.F., Ferm, M., Ortiz, A., et al., 2016. Air pollution trends in the EMEP region between 1990 and 2012. Joint Report of the EMEP Task Force on Measurements and Modelling (TFMM), Chemical Co-ordinating Centre (CCC), Meteorological Synthesizing Centre-East (MSC-E), Meteorological Synthesizing Centre-West (MSC-W).

De Marco, A., Sicard, P., Fares, S., Tuovinen, J.-P., Anav, A., Paoletti, E., 2016. Assessing the role of soil water limitation in determining the Phytotoxic Ozone Dose (PODY) thresholds. Atmos. Environ. 147, 88–97.

Dell'Aquila, A., Mariotti, A., Bastin, S., Calmanti, S., Cavicchia, L., Deque, M., et al., 2016. Evaluation of simulated decadal variations over the Euro-Mediterranean region from ENSEMBLES to Med-CORDEX. Clim. Dyn. 1–20.

Emberson, L., Ashmore, M., Cambridge, H., Simpson, D., Tuovinen, J.-P., 2000. Modelling stomatal ozone flux across Europe. Environ. Pollut. 109, 403–413.

Fares, S., Vargas, R., Detto, M., Goldstein, A.H., Karlik, J., Paoletti, E., et al., 2013. Tropospheric ozone reduces carbon assimilation in trees: estimates from analysis of continuous flux measurements. Glob. Chang. Biol. 19, 2427–2443.

Fu, Y.H., Piao, S., Delpierre, N., Hao, F., Hänninen, H., Liu, Y., et al., 2017. Larger temperature response of autumn leaf senescence than spring leaf-out phenology. Glob. Chang. Biol. 24, 2159–2168.

Fuhrer, J., Skärby, L., Ashmore, M.R., 1997. Critical levels for ozone effects on vegetation in Europe. Environ. Pollut. 97, 91–106.

Guenther, A., Karl, T., Harley, P., Wiedinmyer, C., Palmer, P.I., Geron, C., 2006. Estimates of global terrestrial isoprene emissions using MEGAN (Model of Emissions of Gases and Aerosols from Nature). Atmos. Chem. Phys. 6, 3181–3210. https://doi.org/10.5194/acp-6-3181-2006, 2006.

Guenther, A., Jiang, X., Heald, C., Sakulyanontvittaya, T., Duhl, T., Emmons, L., et al., 2012. The Model of Emissions of Gases and Aerosols From Nature Version 2.1 (MEGAN2. 1): An Extended and Updated Framework for Modeling Biogenic Emissions.

Hendriks, C., Forsell, N., Kiesewetter, G., Schaap, M., Schoepp, W., 2016. Ozone concentrations and damage for realistic future European climate and air quality scenarios. Atmos. Environ. 144, 208–219.

Karlsson, P.E., Klingberg, J., Engardt, M., Andersson, C., Langner, J., Karlsson, G.P., et al., 2017. Past, present and future concentrations of ground-level ozone and potential impacts on ecosystems and human health in northern Europe. Sci. Total Environ. 576, 22–35.

Klingberg, J., Engardt, M., Uddling, J., Karlsson, P., Pleijel, H., 2011. Ozone risk for vegetation in the future climate of Europe based on stomatal ozone uptake calculations. Tellus A 63, 174–187.

Klingberg, J., Engardt, M., Karlsson, P.E., Langner, J., Pleijel, H., 2014. Declining ozone exposure of European vegetation under climate change and reduced precursor emissions. Biogeosciences 11, 5269–5283.

Liu, Q., Fu, Y.H., Zeng, Z., Huang, M., Li, X., Piao, S., 2016a. Temperature, precipitation, and insolation effects on autumn vegetation phenology in temperate China. Glob. Chang. Biol. 22, 644–655.

Liu, Q., Fu, Y.H., Zhu, Z., Liu, Y., Liu, Z., Huang, M., et al., 2016b. Delayed autumn phenology in the Northern Hemisphere is related to change in both climate and spring phenology. Glob. Chang. Biol. 22, 3702–3711.

Madronich, S., 2014. Atmospheric chemistry: ethanol and ozone. Nat. Geosci. 7, 395–397.

Mareckova, K., Wankmueller, R., Pazdernik, K., Purzner, M., Zechmeister, A., Joebstl, R., et al., 2014. Inventory Review 2014, Review of Emission Data Reported Under the LRTAP Convention and NEC Directive Stage 1 and 2 Review, Status of Gridded Data and LPS Data. Umweltbundesamt GmbH, Vienna (ISBN 978-3-99004-095-9).

Mariotti, A., Pan, Y., Zeng, N., Alessandri, A., 2015. Long-term climate change in the Mediterranean region in the midst of decadal variability. Clim. Dyn. 44, 1437–1456.

Menut, L., Bessagnet, B., Khvorostyanov, D., Beekmann, M., Blond, N., Colette, A., et al., 2013. CHIMERE 2013: a model for regional atmospheric composition modelling. Geosci. Model Dev. 6, 981–1028.

Mills, G., Hayes, F., Simpson, D., Emberson, L., Norris, D., Harmens, H., et al., 2011. Evidence of widespread effects of ozone on crops and (semi-) natural vegetation in Europe (1990–2006) in relation to AOT40-and flux-based risk maps. Glob. Chang. Biol. 17, 592–613.

Monks, P.S., Archibald, A., Colette, A., Cooper, O., Coyle, M., Derwent, R., et al., 2015. Tropospheric ozone and its precursors from the urban to the global scale from air quality to short-lived climate forcer. Atmos. Chem. Phys. 15, 8889–8973.

Musselman, R.C., Lefohn, A.S., Massman, W.J., Heath, R.L., 2006. A critical review and analysis of the use of exposure-and flux-based ozone indices for predicting vegetation effects. Atmos. Environ. 40, 1869–1888.

Myneni, R.B., Keeling, C., Tucker, C.J., Asrar, G., Nemani, R.R., 1997. Increased plant growth in the northern high latitudes from 1981 to 1991. Nature 386, 698.

Nemani, R.R., Keeling, C.D., Hashimoto, H., Jolly, W.M., Piper, S.C., Tucker, C.J., et al., 2003. Climate-driven increases in global terrestrial net primary production from 1982 to 1999. Science 300, 1560–1563.

Paoletti, E., Manning, W.J., 2007. Toward a biologically significant and usable standard for ozone that will also protect plants. Environ. Pollut. 150, 85–95.

Piao, S., Fang, J., Zhou, L., Ciais, P., Zhu, B., 2006. Variations in satellite-derived phenology in China's temperate vegetation. Glob. Chang. Biol. 12, 672–685.

Piao, S., Friedlingstein, P., Ciais, P., Viovy, N., Demarty, J., 2007. Growing season extension and its impact on terrestrial carbon cycle in the Northern Hemisphere over the past 2 decades. Glob. Biogeochem. Cycles 21.

Piao, S., Tan, J., Chen, A., Fu, Y.H., Ciais, P., Liu, Q., et al., 2015. Leaf onset in the northern hemisphere triggered by daytime temperature. Nat. Commun. 6.

Pinzon, J.E., Tucker, C.J., 2014. A non-stationary 1981–2012 AVHRR NDVI3g time series. Remote Sens. 6, 6929–6960.

Proietti, C., Anav, A., De Marco, A., Sicard, P., Vitale, M., 2016. A multi-sites analysis on the ozone effects on Gross Primary Production of European forests. Sci. Total Environ. 556, 1–11.

Shen, M., Tang, Y., Chen, J., Yang, X., Wang, C., et al., 2014. Earlier-season vegetation has greater temperature sensitivity of spring phenology in northern hemisphere. PLoS One 9.

Sicard, P., Coddeville, P., Galloo, J.-C., 2009. Near-surface ozone levels and trends at rural stations in France over the 1995–2003 period. Environ. Monit. Assess. 156, 141–157.

Sicard, P., Augustaitis, A., Belyazid, S., Calfapietra, C., de Marco, A., Fenn, M., et al., 2016a. Global topics and novel approaches in the study of air pollution, climate change and forest ecosystems. Environ. Pollut. 213, 977–987.

Sicard, P., De Marco, A., Dalstein-Richier, L., Tagliaferro, F., Renou, C., Paoletti, E., 2016b. An epidemiological assessment of stomatal ozone flux-based critical levels for visible ozone injury in Southern European forests. Sci. Total Environ. 541, 729–741.

Sicard, P., Serra, R., Rossello, P., 2016c. Spatiotemporal trends in ground-level ozone concentrations and metrics in France over the time period 1999–2012. Environ. Res. 149, 122–144.

Simpson, D., Ashmore, M.R., Emberson, L., Tuovinen, J.-P., 2007. A comparison of two different approaches for mapping potential ozone damage to vegetation. A model study. Environ. Pollut. 146, 715–725.

Sitch, S., Cox, P., Collins, W., Huntingford, C., 2007. Indirect radiative forcing of climate change through ozone effects on the land-carbon sink. Nature 448, 791–794.
Skamarock, W.C., Klemp, J.B., Dudhia, J., Gill, D.O., Barker, D.M., et al., 2008. A Description of the Advanced Research WRF Version 3. National Center For Atmospheric Research Boulder Co Mesoscale and Microscale Meteorology Div.
Tai, A.P., Martin, M.V., Heald, C.L., 2014. Threat to future global food security from climate change and ozone air pollution. Nat. Clim. Chang. 4, 817–821.
Tröltzsch, K., Van Brusselen, J., Schuck, A., 2009. Spatial occurrence of major tree species groups in Europe derived from multiple data sources. For. Ecol. Manag. 257, 294–302.
Tuovinen, J.-P., Simpson, D., Emberson, L., Ashmore, M., Gerosa, G., 2007. Robustness of modelled ozone exposures and doses. Environ. Pollut. 146, 578–586.
UNECE, 2017. Mapping Critical Levels for Vegetation. International Cooperative Programme on Effects of Air Pollution on Natural Vegetation and Crops, Bangor, UK.
Wittig, V.E., Ainsworth, E.A., Naidu, S.L., Karnosky, D.F., Long, S.P., 2009. Quantifying the impact of current and future tropospheric ozone on tree biomass, growth, physiology and biochemistry: a quantitative meta-analysis. Glob. Chang. Biol. 15, 396–424.
Wolkovich, E.M., Cook, B.I., Allen, J.M., Crimmins, T.M., Betancourt, J.L., Travers, S.E., et al., 2012. Warming experiments underpredict plant phenological responses to climate change. Nature 485, 494–497.
Zeng, H., Jia, G., Epstein, H., 2011. Recent changes in phenology over the northern high latitudes detected from multi-satellite data. Environ. Res. Lett. 6.
Zhu, Z., Piao, S., Myneni, R.B., Huang, M., Zeng, Z., Canadell, J.G., et al., 2016. Greening of the Earth and its drivers. Nat. Clim. Chang. 6, 791–795.